Optimized polar-azimuthal orientations for polarized light illumination of different superconducting nanowire single-photon detector designs

Massachusetts Institute of Technology

Optimized polar-azimuthal orientations for polarized light illumination of different superconducting nanowire single-photon detector designs

Mária Csete
Áron Sipos
Faraz Najafi
Karl K. Berggren

SPIE

Optimized polar-azimuthal orientations for polarized light illumination of different superconducting nanowire single-photon detector designs

Mária Csete,[a,b] Áron Sipos,[a] Faraz Najafi,[b] and Karl K. Berggren[b]
[a]University of Szeged, Department of Optics and Quantum Electronics,
Dóm tér 9, Szeged, H-6720, Hungary
mcsete@physx.u-szeged.hu
[b]Massachusetts Institute of Technology, Research Laboratory of Electronics,
77 Massachusetts Avenue, Cambridge, Massachusetts 02139

Abstract. The optimum orientations were determined for polarized light illumination of three superconducting nanowire single-photon detector (SNSPD) designs consisting of niobium-nitride (NbN) stripes with dimensions according to conventional devices in 200 nm periodic pattern: (1) standing in air (bare-SNSPD), (2) below ~quarter-wavelength hydrogen-silsesquiox-ane (HSQ) filled nano-cavity (DC-SNSPD), and (3) below HSQ-filled nano-cavity closed by a thin gold reflector (OC-SNSPD). Computations showed that the optical response and near-field distribution vary significantly with polar angle φ, and these variations are analogous across all azimuthal angles γ, but are fundamentally different in different device designs. Larger absorptance is attainable due to p-polarized illumination of NbN patterns in P-orientation, while s-polarized illumination results in higher absorptance in S-orientation. As a result of p-polarized illumination, a global NbN absorptance maximum appears in bare-SNSPD at polar angle corresponding to attenuated total internal reflection (ATIR); in DC-SNSPD exactly at total internal reflection (TIR); and at perpendicular incidence in OC-SNSPD. S-polarized illumination results in a global NbN absorptance maximum in bare-SNSPD at TIR; in DC-SNSPD at polar angle corresponding to ATIR phenomenon; while large and almost polar angle independent absorptance is attainable in OC-SNSPD at small tilting. © *2012 Society of Photo-Optical Instrumentation Engineers (SPIE).* [DOI: 10.1117/1.JNP.6.063523]

1 Introduction

The conventional absorbing structure in superconducting nanowire single-photon detectors (SNSPD) consists of 4-nm-thick niobium-nitride (NbN) stripes having a width of ~30 to 100 nm.[1,2] To ensure an appropriate resistive barrier across the boustrophedonic NbN pattern, wires in 200 nm periodic structure with 50% fill-factor are ideal.

The optimization of SNSPDs requires the maximization of NbN patterns' absorptance. Two different approaches capable of realizing this purpose were described in the literature. The first approach is device design development, which is focused on the design of integrated patterns with the potential to reach larger absorptance in SNSPDs.[3–6] Devices consisting of absorbing NbN stripes aligned below an optical cavity are denominated as OC-SNSPDs.[3,4] Detection efficiency of ~50% was experimentally observed, when OC-SNSPDs consisting of NbN pattern below HSQ-filled optical cavity closed by a 120-nm-thick gold reflector were illuminated perpendicularly by 1550 nm wavelength light.[3]

More complex integrated SNSPD devices consisting of noble-metal nano-antenna-arrays were studied previously both experimentally and theoretically, but only for illumination by

perpendicularly incident light. Applying these integrated devices ∼96% absorptance is attainable, when the **E**-field oscillation direction is perpendicular to the gold pattern.[5,6]

The second approach is device illumination direction optimization. The absorptance of thin lossy wires depends on the relative orientation of their long-axes with respect to **E**-field oscillation direction.[7] Theoretical studies on perpendicular illumination of NbN patterns embedded into dielectric media confirmed that larger absorptance is attainable in the case of **E**-field oscillation direction parallel to the wires.[8,9]

During the description of polarized light illumination we refer to an arrangement as *P*- or *S*-orientation, depending on whether the incidence plane is parallel or perpendicular to the NbN wire-grating. The latest results in the literature proved that *s*-polarized illumination of SNSPD devices at polar angle corresponding to total internal reflection (TIR) is capable of resulting in ∼100% and zero absorptance, when the periodic NbN pattern is in *S*- and *P*-orientation.[10,11]

The purpose of the present study was a systematic investigation of the simplest SNSPD designs to determine the optimal conditions for polarized, substrate side, and off-axes illumination in conical-mounting. Inspection of illumination direction-dependent nano-optical phenomena enables the maximization of absorptance in fundamentally different orientations of different device designs. Similar studies were realized for nano-cavity-array integrated SNSPDs, which are described in our work elsewhere.[12]

2 Theoretical Methods

Three types of SNSPD designs were studied theoretically, where the 200 nm periodic pattern of 4-nm-thick and 100-nm-wide NbN stripes, which are covered by a ∼2-nm-thick NbNO$_x$ layer is: (1) standing in air [bare-SNSPD, Fig. 1(a)]; (2) arrayed below 279-nm-thick, i.e., ∼quarter-wavelength HSQ-filled nano-optical cavity [DC-SNSPD, Fig. 1(b)]; and (3) integrated with analogous HSQ-cavity covered by a 60-nm-thick gold reflector [OC-SNSPD, Figure 1(c)].

2.1 Finite Element Method to Determine the Optical Response and Near-Field Distribution

The three-dimensional finite element method (FEM) developed in our previous work based on the radio frequency module of Comsol Multiphysics software package (COMSOL AB) was
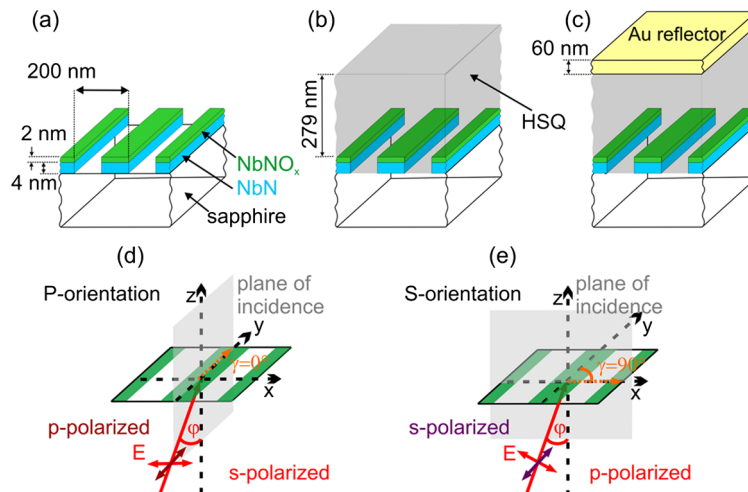

Fig. 1 Schematic drawings of the device designs studied consisting of 200 nm periodic pattern of 4-nm-thick and 100-nm-wide NbN stripes covered by ∼2 nm NbNO$_x$ layer: (a) standing in air (bare-SNSPD); (b) arrayed below HSQ-filled nano-cavity with 279 nm length (DC-SNSPD); and (c) integrated with HSQ-cavity covered by a 60-nm-thick Au reflector (OC-SNSPD). All patterns are illuminated by *p*- and *s*-polarized $\lambda = 1550$ nm light, the illumination directions in conical mounting are specified by φ polar and γ azimuthal angles. The two specific orientations studied in more detail are: (d) *P*-orientation ($\gamma = 0$ deg), and (e) *S*-orientation ($\gamma = 90$ deg).

applied.[11] Special 3D FEM models were used to determine the effect of polar and azimuthal illumination angles on the optical response and to map the electromagnetic near-field distribution at specific orientations corresponding to extrema on NbN absorptance.

The absorptance was determined based on Joule-heating inside NbN and gold segments, while reflectance and transmittance signals were extracted based on power-outflows from the studied models.

In a coarse dual-angle-dependent study, the φ polar angle and the γ azimuthal orientation were varied within the ranges of $\varphi = [0 \text{ deg}, 85 \text{ deg}]$ and $\gamma = [0 \text{ deg}, 90 \text{ deg}]$ with resolution of $\Delta\varphi = \Delta\gamma = 5$ deg [Figs. 1(d), 1(e), 2, and 3]. The special configurations of p- and s-polarized illumination of integrated patterns in P-orientation ($\gamma = 0$ deg) and in S-orientation ($\gamma = 90$ deg) were investigated with $\Delta\varphi = 1$ deg resolution across the entire $\varphi = [0 \text{ deg}, 85 \text{ deg}]$ region. In intervals surrounding the NbN absorptance maxima the polar angle was varied with larger $\Delta\varphi = 0.05$ deg resolution (Figs. 4 and 5).

2.2 Transfer Matrix Method to Determine the Optical Response

Complementary transfer matrix method (TMM) calculations were performed on different multi-layers composing the vertical stacks in device designs shown in Fig. 1(a) to 1(c).[13] The absorptance, reflectance, and transmittance were determined by weighting the optical responses of NbN-containing and NbN-free stacks according to their corresponding 50% fill-factor.[11] These results were compared with the results of FEM computations to determine the origin of extrema appearing on the optical response (Figs. 4 and 5).

3 Optical Response of Different SNSPD Device Designs

The common characteristics of optical responses in all three device designs are that off-axes illumination results in significant variation as a function of φ polar angle (Figs. 2 to 6), while only a slow monotonous variation is observable, when γ azimuthal angle is tuned (Figs. 2 and 3). As a result, the extrema are analogous, however, the maximal values differ in P- and S-orientations (Figs. 2 to 5). This difference could be observed only via FEM, caused by inherent limits of TMM, which method cannot account for absorption modification occurring, when the plane of incidence is rotated with respect to the long-axes of NbN stripes.[11]

3.1 Dual-Angle-Dependent NbN Absorptance Resulted by p-Polarized Light Illumination

In case of p-polarized light illumination, the P-orientation of NbN patterns results in larger absorptance in all of the three studied device designs through the entire polar angle interval (Fig. 2). The absorptance maxima appear in entirely different polar angle intervals in different device designs [Figs. 2, 4, and 6(a); Table 1], their origin will be described in Secs. 3.3 and 4.1.

Figure 2(a) indicates that the dual-angle-dependent absorptance of NbN pattern in bare-SNSPD exhibits a narrow minimum in the interval of TIR at all azimuthal angles, similarly to the results in Ref. 10.
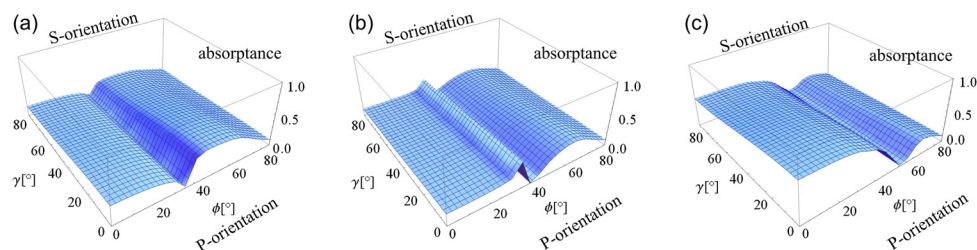

Fig. 2 Dual-angle-dependent absorptance due to p-polarized illumination of NbN patterns in (a) bare-SNSPD, (b) DC-SNSPD, and (c) OC-SNSPD.

In DC-SNSPD the dual-angle-dependent absorptance indicates a global maximum at TIR [Fig. 2(b)], i.e., the curve is more similar at all azimuthal angles to the polar-angle-dependent absorptance presented previously for *s*-polarized illumination of NbN structures in *S*-orientation in Ref. 10.

In OC-SNSPD the fundamental advantage of gold reflector is that the absorptance is enhanced at perpendicular incidence and throughout experimentally more easily implementable small polar angles [Fig. 2(c)].[11]

3.2 *Dual-Angle-Dependent NbN Absorptance Resulted by s-Polarized Light Illumination*

In case of *s*-polarized illumination, larger absorptance is attainable through all polar angles in all of the three studied device designs, when the NbN structure is in *S*-orientation (Fig. 3). The absorptance maxima appear in slightly different polar angle intervals in different devices (Table 1), their origin will be described in Secs. 3.4 and 4.2.

Figure 3(a) indicates that the dual-angle-dependent absorptance of bare-SNSPD exhibits a global maximum exactly at the polar angle corresponding to TIR at all azimuthal angles, analogously with Ref. 10.

In DC-SNSPS, the dual-angle-dependent absorptance indicates a broadened maximum shifted to larger polar angles at all azimuthal angles [Fig. 3(b)].

In OC-SNSPD, uniform and strongly enhanced absorptance signal is observable from perpendicular incidence throughout large polar angles, but the maximal values are somewhat smaller than in bare- and DC-SNSPDs [Fig. 3(c)].

3.3 *Polar-Angle-Dependent Optical Responses Resulted by p-Polarized Light Illumination*

The high resolution computations show that sudden changes are observable at the polar angle corresponding to TIR in all studied device designs (Fig. 4).
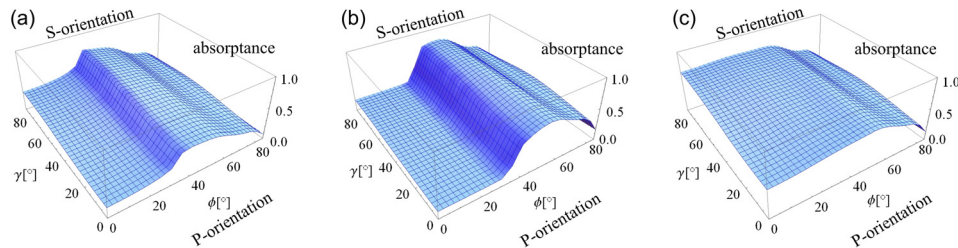

Fig. 3 Dual-angle-dependent absorptance due to *s*-polarized light illumination of NbN patterns in (a) bare-SNSPD, (b) DC-SNSPD, and (c) OC-SNSPD.
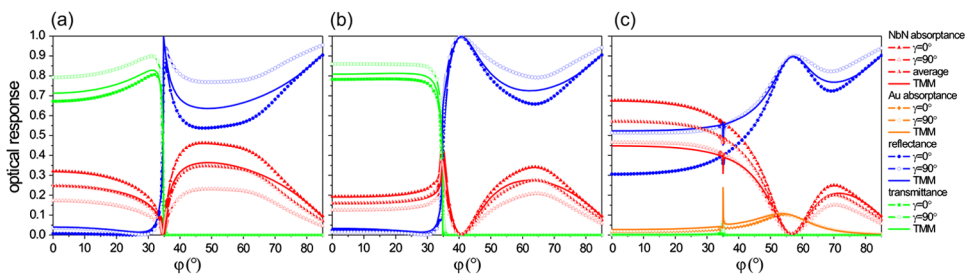

Fig. 4 The comparison of optical responses in *P*-orientation ($\gamma = 0$ deg, closed symbols) and in *S*-orientation ($\gamma = 90$ deg, open symbols) determined by FEM with optical responses determined by TMM (lines) for the case of *p*-polarized light illumination of NbN patterns in (a) bare-SNSPD, (b) DC-SNSPD, and (c) OC-SNSPD.

Figure 4(a) shows that at perpendicular incidence, the absorptance in *P*-orientation is larger than the TMM-absorptance, and approximately two times larger than the absorptance in *S*-orientation.[11] A global minimum is observable on the absorptance curves in both orientations at 34.7 deg corresponding to TIR, in accordance with the zero absorptance predicted by TMM and in the literature.[10] The global maxima are at ∼48 deg and 49 deg polar angles, where the absorptance reaches 46.3% and 23.1% value in *P*- and *S*-orientation, respectively, due to NbN-related ATIR. Based on these observations the optimal orientation of bare-SNSPD is *P*-orientation and tilting at 48 deg polar angle.

Even though the transmittance indicates a cut-off at TIR, the reflectance exhibits ATIR phenomenon according to presence of lossy NbN pattern at large polar angles, where light in-coupling into the device would require a special method. The FEM absorptance is significantly larger in *P*-orientation than the TMM absorptance through the entire polar-angle interval, while the average of FEM absorptances equals with the TMM absorptance.

Figure 4(b) presents that in DC-SNSPD the absorptance values at perpendicular incidence are smaller than in analogous arrangements of bare-SNSPD. Then the absorptance increases, and reaches a global maximum at 34.8 deg incidence corresponding to TIR. The enhanced 43.1% and 31.3% absorptances at this tilting in *P*- and *S*-orientation are larger than the absorptances at perpendicular incidence on either of bare- and DC-SNSPDs. Further tilting of DC-SNSPD is not advantageous, since the absorptance indicates a global minimum at 41 deg, then local maxima originating from NbN-related ATIR appear at 64 deg, where the absorptance values are only slightly larger than at perpendicular incidence on bare- or DC-SNSPDs in analogous arrangements.

The transmittance indicates a cut-off at 34.8 deg polar angle, while the reflectance curve shows a Brewster-like minimum at ∼29 deg, followed by an inflection point at 34.8 deg. The total reflectance is shifted to 41 deg in presence of HSQ layer, and the reflectance exhibits ATIR characteristics at large polar angles caused by presence of lossy NbN stripes. The FEM absorptance in *P/S*-orientation is only slightly larger/smaller, than the TMM absorptance, and the average of FEM signals equals with the TMM absorptance across all polar angles. The TMM absorptance curve indicates an analogous global maximum at 34.8 deg, however, this method predicts smaller maximal absorptance.

Figure 4(c) indicates that small polar angles are the most appropriate for detection, when OC-SNSPD is illuminated by *p*-polarized light. The highest available absorptance observed at perpendicular incidence is 67.6% in *P*-orientation, which value is approximately 1.5 times larger than the 46.5% observed in *S*-orientation.[11] There are narrow local NbN absorptance minima at 35.05 deg polar angle, originating from gold-related ATIR phenomenon. Significantly broader global minimum appears at 57 deg, which is followed by a small local maximum at ∼70 deg in both orientations originating from NbN-related ATIR.

The gold reflector's absorptance indicates a narrow local maximum at 35.15 deg and broad global maxima at 55 deg and 53 deg incidence angles in *P*- and *S*-orientations, confirming that the minima in NbN absorptance are in those polar angle intervals, where TIR is frustrated caused by losses in gold. These orientations result in surface plasmon polariton excitation at air-gold and at HSQ-gold boundary.[11] The transmittance is suppressed in the entire polar angle interval in OC-SNSPD; only a slight transmittance is observable at 35.05 deg. The average of FEM signals significantly differs from TMM responses, namely in *S*-orientation the absorptance approximates it through the entire polar angle interval, while in *P*-orientation the absorptance is considerably larger throughout the global minimum.

The OC-SNSPD might be considered as a grating-waveguide configuration, which supports polar-angle-dependent Fabry-Perrot resonances.[14] This explains the pronounced effect of tilting on the optical response.

3.4 *Polar-Angle-Dependent Optical Responses Resulted by s-Polarized Light Illumination*

The high resolution computations show that the maxima surround the polar angle corresponding to TIR in all of the three studied SNSPD device designs (Fig. 5).
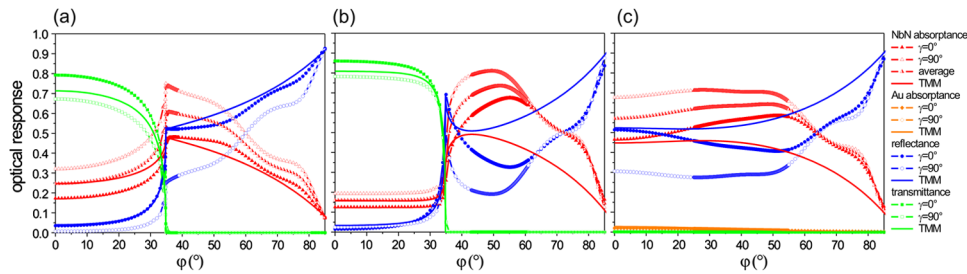
Fig. 5 The comparison of optical responses in *P*-orientation ($\gamma = 0$ deg, closed symbols) and in *S*-orientation ($\gamma = 90$ deg, open symbols) computed by FEM with optical responses determined by TMM (lines) for the case of *s*-polarized light illumination of NbN patterns in (a) bare-SNSPD, (b) DC-SNSPD, and (c) OC-SNSPD.

Figure 5(a) shows that the TIR phenomenon entirely governs the optical response of bare-SNSPD. At perpendicular incidence, the absorptance is approximately two times larger in *S*-than in *P*-orientation, i.e., the ratio is reversed compared to *p*-polarized illumination. The absorptance indicates global maxima of 75% and 47.9% at 34.85 and 34.75 deg in *S*- and *P*-orientations, respectively, then monotonously decreases. The optimal orientation for *s*-polarized light illumination of bare-SNSPD is *S*-orientation and tilting at polar angle corresponding to TIR.

Although the transmittance indicates a cut-off at TIR, the reflectance monotonously increases above 34.85 deg, limiting the available NbN absorptance. The average of FEM absorptances equals with the TMM absorptance through TIR, above TIR the NbN absorptance in *P*-orientation approximates the TMM absorptance, while it is considerably larger in *S*-orientation. The absorptance is enhanced in *s*-to-*S* configuration due to the parallelism of the **E**-field oscillation to the NbN stripes [Fig. 1(e)].

Figure 5(b) presents that ATIR phenomenon governs the optical responses through wide φ interval during *s*-polarized illumination of DC-SNSPD. In the case of perpendicular incidence the absorptance is slightly larger in *S*-orientation than in *P*-orientation. The global absorptance maxima originating from NbN-related ATIR appear at 49.4 deg and 55.15 deg, with values of 80.9% in *S*- and 67.3% in *P*-orientation, respectively. These maximal values are larger than the absorptance maxima observed on bare-SNSPD. The optimal orientation for *s*-polarized illumination of DC-SNSPD is *S*-orientation at polar angle corresponding to ATIR.

Even though the transmittance indicates a cut-off at 34.85 deg, the reflectance curve exhibits NbN-related ATIR characteristic in DC-SNSPD at large polar angles. The average of FEM signals equals with TMM absorptance through TIR, but is considerably larger across polar angles above TIR. The FEM prediction regarding the advantage of ATIR is in agreement with TMM results, but TMM predicts smaller absorptance at smaller polar angle.

Figure 5(c) indicates slowly varying optical responses with polar angle tuning, when OC-SNSPD is illuminated by *s*-polarized light. At perpendicular incidence, the absorptance is ~1.5 times larger in *S*-orientation, i.e., the ratio is reversed compared to *p*-polarized illumination. The 71.3% global maximum appears before TIR at 27.85 deg in *S*-orientation, while considerably smaller value of 58.5% is observable at larger 51.5 deg polar angle in *P*-orientation, i.e., in the interval corresponding to ATIR.

Although the gold absorptance does not indicate any extrema, it monotonously decreases, and the transmittance is negligible through the entire polar angle interval, the reflectance monotonously increases and limits the available NbN absorptance. FEM predicts considerably larger absorptance in both arrangements through the entire interval than TMM.

3.5 *Comparison of Different Optical Systems Illuminated by Polarized Light*

The fundamentally different absorptances available in different device designs are compared in Figs. 6(a) and 6(b) and Table 1 for the optimum *P/S*-orientations of NbN pattern in the case of *p/s*-polarized light illumination.

Figure 6(a) indicates that the highest NbN absorptance is attainable in OC-SNSPD in a wide interval of small polar angles, but it is possible to enhance the absorptance already without a gold
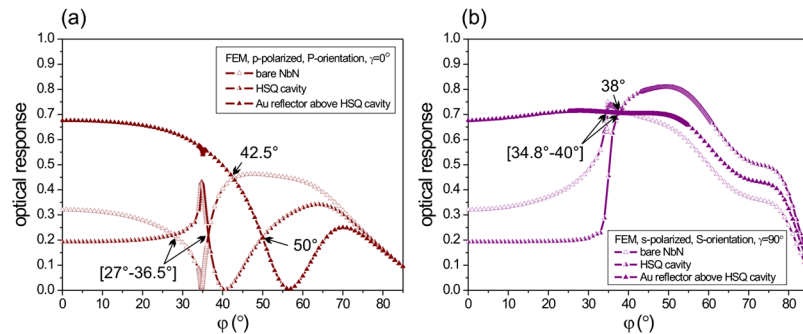
Fig. 6 Comparison of polar-angle-dependent absorptance in three device designs for the case of (a) *p*-polarized illumination of NbN patterns in *P*-orientation and (b) *s*-polarized light illumination of NbN patterns in *S*-orientation.

Table 1 Summary of NbN absorptance values observed at perpendicular incidence, governed by TIR and NbN-related ATIR phenomenon on the polar-angle-dependent absorptance of three device designs, when the NbN pattern in *P/S*-orientation is illuminated by *p/s*-polarized light. The absorptances at optimal orientations are emphasized with numbers in bold.

Tilting		*P*-orientation			*S*-orientation		
	Media	air	HSQ	Au + HSQ	air	HSQ	Au + HSQ
Perpendicular	φ (deg)	0	0	0	0	0	0
	A	0.32	0.193	**0.676**	0.32	0.193	**0.676**
TIR	φ (deg)	34.7	34.75	35.05	34.85	—	27.85
	A	0.01	**0.43**	0.539	**0.75**	—	0.71
NbN	φ (deg)	48	64	70	—	49.4	44.7
	A	**0.463**	0.341	0.25	—	**0.809**	0.703

cover layer throughout the [27 deg to 36.5 deg] polar angle interval in *P*-orientation of DC-SNSPD. In OC-SNSPD the absorptance is larger than in bare-SNSPD through 42.5 deg incidence angle, while the curve crosses the absorptance of DC-SNSPD at 50 deg polar angle.

The comparison of absorptances achieved when different SNSPD devices are illuminated by *s*-polarized light indicates that it is possible to maximize absorptance by aligning NbN patterns in *S*-orientation in DC-SNSPD, and tilting at polar angle larger than 38 deg, as shown in Fig. 6(b). Interestingly, the absorptance is larger in [34.8 deg to 40 deg] polar angle interval in bare-SNSPD than in OC-SNSPD. The advantage of the gold reflector is that it results in the most uniformly enhanced absorptance through a wide interval of small polar angles in OC-SNSPD.

4 Near-Field Phenomena of Different SNSPD Device Designs

To understand the origin of NbN absorptance extrema, the near-field phenomena were also inspected. The main characteristic is that the **E**-field distribution is symmetrical along the cross-sections perpendicular to NbN stripes in *P*-orientation, while it is asymmetrical in *S*-orientation [Figs. 7(d) to 7(f) and 7(g) to 7(i); and 8(d) to 8(f) and 8(g) to 8(i)], in accordance with different relative orientations of the intensity modulation originating from off-axis illumination with respect to the NbN patterns.

Interestingly, the maximal **E**-field values are larger at analogous polar angles in the case of *p*-to-*S* and *s*-to-*P* configurations in all device designs, but the external **E**-field enhancement is accompanied by less effective penetration [Figs. 7(g) to 7(i), and 8(d) to 8(f)].

The resistive heating correlates with the NbN absorptance, i.e., larger averaged Joule-heating is observable inside the absorbing NbN segments in *p*-to-*P* and *s*-to-*S* configurations, and the highest averaged values are observable at the global maxima on the absorptance [Figs. 7(j–l)and 8(j–l), red-to-blue curves]. Although the maximal values are similar, the resistive heating distribution is significantly different in *P*- and *S*-orientations.

4.1 *Near-Field Phenomena Accompanying p-Polarized Light Illumination*

In bare-SNSPD the most intensive **E**-field penetrating into NbN stripes is due to evanescent-field concentration accompanying the ATIR phenomenon at the global maxima [Fig. 7(d) and 7(g)]. The more homogeneous **E**-field distribution surrounding the NbN segments ensures attainment of the highest absorptance at 48 deg polar angle in *P*-orientation [Fig. 7(d)].

The comparison of resistive heating line cross-sections proves that more effective and compensated penetration occurs at the global maximum in *P*-orientation [Fig. 7(j)].

Figure 7(e) and 7(h) shows that in DC-SNSPD the incoming and reflected **E**-fields are in phase around the NbN stripes due to the phase-shift introduced by HSQ cavity at TIR. The maximal resistive heating is slightly larger in *S*-orientation, but the NbN segments are more uniformly heated in *P*-orientation [Fig. 7(k)].
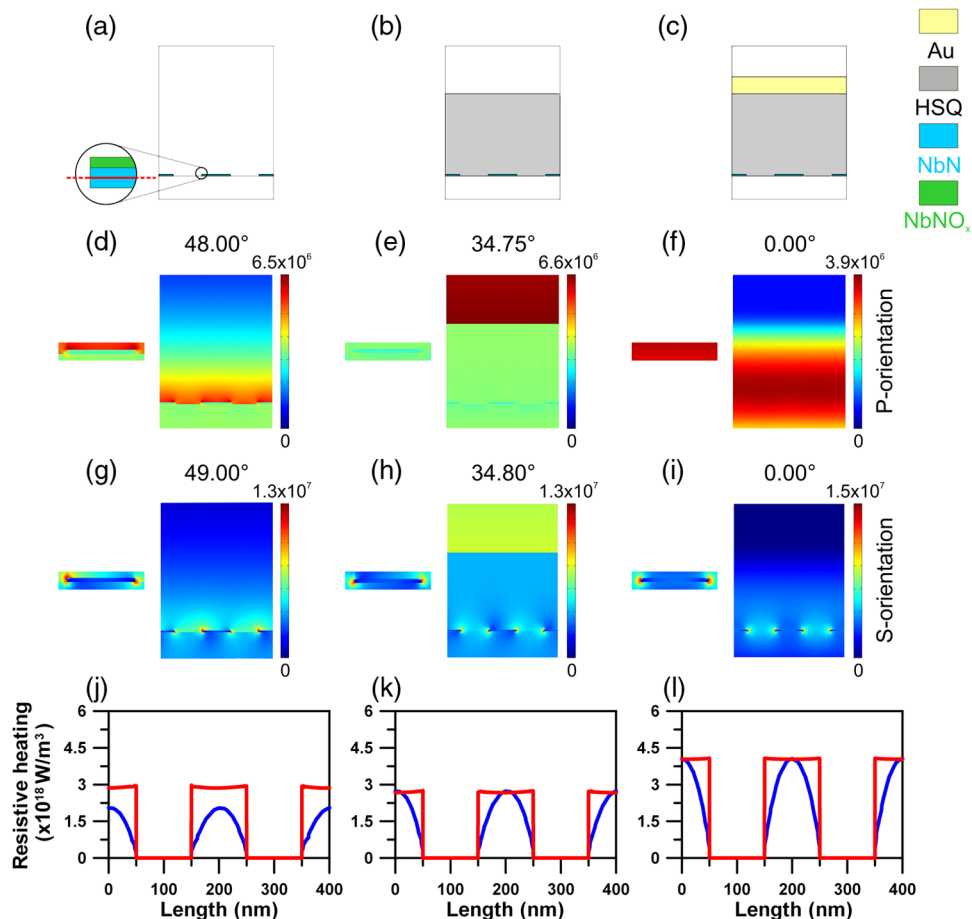

Fig. 7 (a) to (c) Schematic drawing showing two unit cells in a plane perpendicular to the 200 nm periodic NbN pattern, where the near-field cross-sections are investigated around NbN pattern in: (a), (d), (g), and (j) bare-SNSPD; (b), (e), (h), and (k) DC-SNSPD; and (c), (f), (i), and (l) OC-SNSPD. The normalized **E**-field distribution due to *p*-polarized light illumination at the extrema observed (d) to (f) in *P*-orientation, and (g) to (i) in *S*-orientation. The time evolution of the **E**-field is also presented for *p*-polarized light illumination in *P*-orientation: (d), (e), and (f) in Media 1, 2, and 3. (j) to (l) The comparison of the resistive heating at the extrema inside NbN segments in *P*-orientation (red) and in *S*-orientation (blue) along the horizontal line indicated on the (a) inset.

Figures 7(f) and 7(i) indicate that at perpendicular incidence there is an **E**-field antinode at the bottom of the HSQ-cavity due to the gold reflector, which explains the very large absorptance in OC-SNSPD. The line cross-sections indicate equal maximal Joule-heating values at perpendicular incidence, with more uniform distribution in *P*-orientation [Fig. 7(l)].

4.2 Near-Field Phenomena Accompanying s-Polarized Light Illumination

On the near-field pictures about *s*-polarized light illuminated NbN pattern in bare-SNSPD, a large **E**-field with continuous phase through the NbN stripes is observable at TIR corresponding to the global absorptance maximum [Fig. 8(d) and 8(g)]. The cross-sections about the resistive heating indicate larger and more uniform heating in *S*-orientation in the NbN stripes [Fig. 8(j)].

In DC-SNSPD, an evanescent **E**-field concentration is observable around the NbN stripes at ATIR-related absorptance maximum, which is further enhanced due to the phase-shift introduced by the HSQ nano-cavity [Fig. 8(e) and 8(h)]. Even though the maximal resistive heating is larger in *P*-orientation, the heating is more compensated in *S*-orientation through the NbN stripes [Fig. 8(k)].
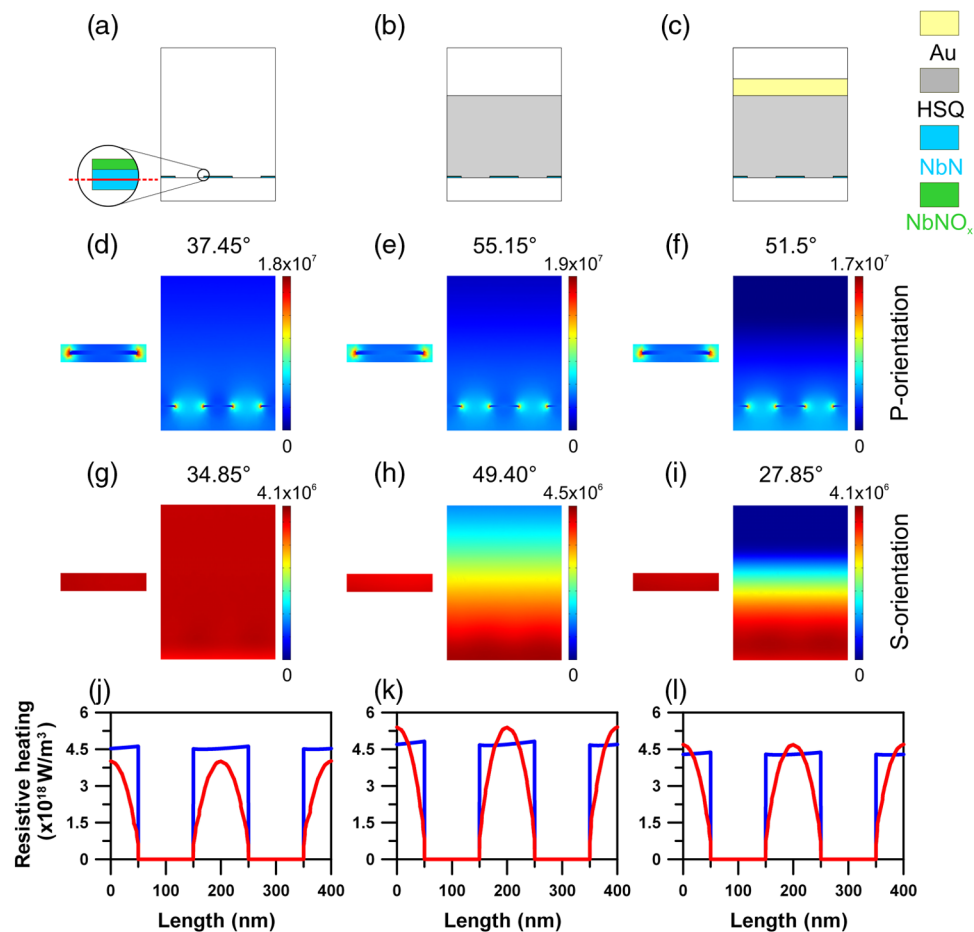

Fig. 8 (a) to (c) Schematic drawing showing two unit cells in a plane perpendicular to the 200 nm periodic NbN pattern, where the near-field cross-sections are investigated around NbN pattern in: (a), (d), (g), and (j) bare-SNSPD; (b), (e), (h), and (k) DC-SNSPD; and (c), (f), (i), and (l) OC-SNSPD. The normalized **E**-field distribution due to *s*-polarized light illumination at the extrema observed (d) to (f) in *P*-orientation, and (g) to (i) in *S*-orientation. The time evolution of the **E**-field is presented for *s*-polarized light illumination in *S*-orientation (g), (h), and (i) in Media 4, 5, and 6. (j) to (l) The comparison of the resistive heating at the extrema inside NbN segments in *P*-orientation (red) and in *S*-orientation (blue) along the horizontal line indicated on the inset in (a).

In OC-SNSPD there is an **E**-field antinode at the bottom of the cavity at both global maxima [Fig. 8(f) and 8(i)]. The resistive heating exhibits the same relation as below the HSQ cavity, with slightly reduced maximal amplitudes [Fig. 8(l)].

5 Conclusion

The most important result of these calculations is that optimization of the illumination direction of absorbing NbN patterns can help to maximize the absorptance of the SNSPDs, indicating that all device designs studied are promising in specific applications.

While the course of dual-angle-dependent variations fundamentally differs in the three SNSPD device designs in the case of specific polarizations, each device design has its optimum illumination conditions. Based on FEM computation results, the optimum azimuthal orientation of the NbN stripes with respect to the incidence plane of polarized light is the P/S-orientation in case of p/s-polarized light illumination. Both correspond to an **E**-field oscillation parallel to the stripes. The optimum polar angles resulting in maximal absorptance were also determined. When p-polarized light is applied for illumination, these orientations are the polar angle resulting in NbN-related ATIR in bare-SNSPD, the polar angle corresponding to TIR in DC-SNSPD, and perpendicular incidence in OC-SNSPD. For s-polarization the global maximum is at TIR in bare-SNSPD, which is shifted to the region of ATIR in DC-SNSPD, and the losses are compensated through a wide interval of small polar angles in OC-SNSPD.

Acknowledgments

References

1. G. N. Gol'tsman et al., "Picosecond superconducting single-photon optical detector," *Appl. Phys. Lett.* **79**(6), 705–708 (2001), http://dx.doi.org/10.1063/1.1388868.
2. F. Marsili et al., "Single-photon detectors based on ultranarrow superconducting nanowires," *Nano Lett.* **11**(5), 2048–2053 (2011), http://dx.doi.org/10.1021/nl2005143.
3. K. M. Rosfjord et al., "Nanowire single-photon detector with an integrated optical cavity and anti-reflection coating," *Opt. Express* **14**(2), 527–534 (2006), http://dx.doi.org/10.1364/OPEX.14.000527.
4. S. Miki et al., "Compactly packaged superconducting nanowire single-photon detector with an optical cavity for multichannel system," *Opt. Express* **17**(226), 23557–235640 (2006), http://dx.doi.org/10.1364/OE.17.023557.
5. X. Hu et al., "Efficiently coupling light to superconducting nanowire single-photon detectors," *IEEE Trans. Appl. Supercond.* **19**(3), 336–340 (2009), http://dx.doi.org/10.1109/TASC.2009.2018035.

6. X. Hu et al., "Superconducting nanowire single-photon detectors integrated with optical nano-antennae," *Opt. Express* **19**(1), 17–31 (2011), http://dx.doi.org/10.1364/OE.19.000017.

7. E. A. Lewis and J. P. Casey, "Electromagnetic reflection and transmission by gratings of resistive wires," *J. Appl. Phys.* **23**(6), 605–608 (1952), http://dx.doi.org/10.1063/1.1702264.

8. E. F. C. Driessen et al., "Impedance model for the polarization-dependent optical absorption of superconducting single-photon detectors," *Eur. J. Appl. Phys.* **47**(1071), 1–6 (2009), http://dx.doi.org/10.1051/epjap/2009087.

9. V. Anant et al., "Optical properties of superconducting nanowire single-photon detectors," *Opt. Express* **16**(14), 10750–10761 (2008), http://dx.doi.org/10.1364/OE.16.010750.

10. E. F. C. Driessen and M. J. A. de Dood, "The perfect absorber," *Appl. Phys. Lett.* **94**(171109), 1–3 (2009), http://dx.doi.org/10.1063/1.3126062.

11. M. Csete et al., "Numerical method to optimize the polar-azimuthal orientation of infrared superconducting nanowire single photon detectors," *Appl. Opt.* **50**(31), 5949–5956 (2011), http://dx.doi.org/10.1364/AO.50.005949.

12. M. Csete et al., "Impact of polar-azimuthal illumination angles on nano-cavity-array integrated superconducting nanowire single-photon detectors efficiency," *Opt. Express* **20**(15), 17065–17081 (2012), http://dx.doi.org/10.1364/OE.20.017065.

13. M. Born and E. Wolf, *Principles of Optics*, Pergamon Press, Cambridge (1964).

14. E. Popov et al., "Enhanced transmission due to nonplasmon resonances in one- and two-dimensional gratings," *Appl. Opt.* **43**(5), 999–1008 (2004), http://dx.doi.org/10.1364/AO.43.000999.

Biographies and photographs of the authors not available.